Transition state dynamics of the OH+OH→O+H_2O reaction studied by dissociative photodetachment of $H_2O_2^-$

Hans-Jürgen Deyerl,[a] Todd G. Clements, A. Khai Luong,[b] and Robert E. Continetti[c]
Department of Chemistry and Biochemistry, University of California, San Diego, La Jolla, California 92093-0340

(Received 30 May 2001; accepted 27 July 2001)

Photoelectron-photofragment coincidence (PPC) spectroscopy has been used to study the dissociative photodetachment of $H_2O_2^-$ and $D_2O_2^-$. The observed partitioning of photoelectron and photofragment translational energies provides information on the dynamics in the transition state region of the reaction between two hydroxyl radicals: $OH+OH\rightarrow O(^3P)+H_2O$. The data reveal vibrationally resolved product translational energy distributions for both the entrance channel OH+OH and the exit channel $O(^3P)+H_2O$ upon photodetachment. The total translational energy distribution shows a convoluted vibrational progression consistent with antisymmetric stretch excitation of H_2O in the exit channel and OH stretch in the entrance channel. The photoelectron spectra are compared to two-dimensional time-dependent wave packet dynamics simulations based on an anharmonic potential in the anion and a model collinear potential energy surface for the neutral complex. The PPC spectra also yield the dissociation energies $D_0(H_2O_2^-\rightarrow H_2O+O^-)=1.15\pm0.08$ eV and $D_0(D_2O_2^-\rightarrow D_2O+O^-)=1.05\pm0.08$ eV. © *2001 American Institute of Physics.* [DOI: 10.1063/1.1404148]

I. INTRODUCTION

Photodetachment from hydrogen bonded anions of the type AHB^- provides a route to the exploration of the transition state region for the corresponding neutral bimolecular reactions A+HB→AH+B. Neumark and co-workers have made substantial progress in characterizing transition states by analysis of the photoelectron spectra of the bound anion precursor AHB^-, where A and B have been both single atoms and molecular groups.[1] Photoelectron-photofragment coincidence (PPC) spectroscopy can extend these studies significantly by allowing characterization of the entire dissociative photodetachment (DPD) event.[2] DPD occurs when removal of an electron from a stable anion produces a neutral in a dissociative or metastable state that undergoes rapid dissociation. For stable negative ions in a nuclear configuration similar to that of the transition state of a bimolecular reaction, photodetachment can be used to access the transition state region. By combining the techniques of photofragment translational spectroscopy and photoelectron spectroscopy, the kinetic energies of the photoelectrons and photofragments can be measured in coincidence, providing a complete kinematic measure of the dynamics of DPD.

In the experiments presented here, the dynamics of DPD in $H_2O_2^-$ and $D_2O_2^-$ have been investigated, and yield insights into the dynamics of the reaction:

$$OH+OH\rightarrow O(^3P)+H_2O. \tag{1}$$

The hydroxyl radical is the predominant oxidant in the troposphere, in combustion processes and in a wide range of other chemically active environments.[3] The reaction between two hydroxyl radicals forming $O(^3P)$ and H_2O is an exothermic reaction ($\Delta E_{r,0\,K}=-0.684$ eV)[4,5] that is a minor source of H_2O in hydrocarbon flames, while the reverse reaction is a chain branching process which results in flame acceleration at higher temperatures.[6] The reverse reaction is also thought to be important in the mechanism of the thermal De–NO_x method for removal of NO_x.[7] In the context of atmospheric chemistry, the reverse reaction serves as a major source of tropospheric OH radicals.[8,9] The hydroxyl radical is also known to play a vital role in stratospheric ozone chemistry through the HO_x cycle.[10] In addition, the reaction is of significant theoretical interest as it corresponds to the association of two open-shell radicals on a potential energy surface (PES) governed by a complicated interplay of long range dipole–dipole and short range valence forces.

Since these studies begin with the $H_2O_2^-$ anion, a brief review of the negative ion chemistry is necessary. Figure 1 shows a schematic energy diagram for the $H_2O_2^-$/OH+OH $+e^-$ system. The anionic reaction

$$OH^-+OH\rightarrow O^-+H_2O \tag{2}$$

has been the subject of a number of studies.[11] The reaction is exothermic by 0.35 eV at 0 K, given the heats of formation $\Delta H_{f,0}$ of OH^-, OH, O^-, and H_2O.[4,12] Ion-molecule reaction studies by Lifshitz[13] and Van Doren *et al.*[14] using isotopically labeled compounds revealed very rapid isotope exchange near the statistical limit showing that at some point the oxygen atoms in the collision complex become equivalent. Lifshitz interpreted this in terms of an asymmetric double-well potential with two distinct isomers $O^-(H_2O)$

[a]Current address: Research Center COM, DTU, DK-2800 Kgs. Lyngby, Denmark.
[b]Current address: Sandia National Laboratories, P.O. Box 969, MS 9056, Livermore, CA 94551.
[c]Author to whom correspondence should be addressed. Electronic mail: rcontinetti@ucsd.edu

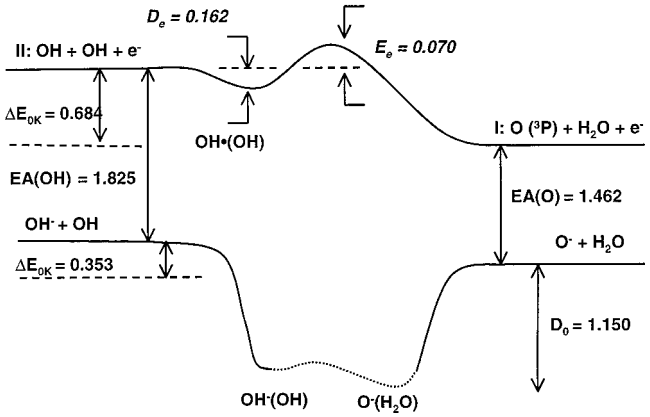

FIG. 1. Energetics diagram for the $H_2O_2^-$/OH+OH system. The potential energy is shown as a function of a generic reaction coordinate. The values in italics are theoretically determined values from Ref. 31.

and $OH^-(OH)$, with $O^-(H_2O)$ complex being the more stable isomer.[13] The bond dissociation energy $D_0(H_2O_2^- \rightarrow H_2O+O^-)$ has been determined experimentally to lie within the range $1.08\,\text{eV} < D_0 < 1.30\,\text{eV}$.[13] Johnson and co-workers studied reaction (2) by photodissociation of O_2^- in the $O_2^-(H_2O)$ cluster anion, observing nearly equal production of O^- and OH^-.[15] There have only been a few theoretical calculations on this system,[11,16–19] which support the double-well potential energy surface with local minima best described as electrostatic ion/dipole complexes [i.e., $O^-(H_2O)$ and $OH^-(OH)$]. The most detailed study by Hrušák *et al.*,[11] however, suggests a potential energy surface (PES) for reaction (2) in which the $OH^-(OH)$ complex is a very shallow minimum or rather a shoulder on the PES. Restricted one-dimensional calculations (variation of the O–H–O distance for the transferred hydrogen atom) on the collinear anion surface were carried out by Neumark and co-workers[20] and found to be consistent with the work of Hrušák *et al.*[11]

The neutral reaction (1) has been the subject of numerous experiments. Measurements of the reaction rate over a wide range of temperatures show that the disproportionation of the hydroxyl radical exhibits non-Arhennius behavior,[9,21] consistent with previous measurements for the reverse reaction.[22] The reason for this non-Arhennius behavior has been debated with respect to the existence of a potential barrier along the reaction path. Wagner and Zellner suggested a barrierless reaction between two OH radicals in which the long-range attractive forces affected the temperature dependence of the reaction.[9] More recent work on the kinetics of this reaction has been carried out over a wide range of temperatures and pressures by Troe and co-workers[23] and by Bedjanian *et al.*[24] The dynamics of the neutral reactions at high levels of vibrational excitation were recently reported by Pfeiffer *et al.*[25] Using overtone excitation, they determined the vibrational and rotational state distribution of OH and OD for the reaction $O(^3P)+HOD(4\nu_{OH})$. In addition, there have been a number of studies, both gas phase and in clusters, of the excited-state reaction $O(^1D)+H_2O$.[26]

For the neutral reaction (1), several *ab initio* calculations on the potential energy surface have been reported due to its importance in the hydrogen oxygen combustion mechanism.[27–29] In a multireference study of the long-range $OH(^2\Pi)+OH(^2\Pi)$ potential, Harding showed that the four singlet surfaces correlating with ground-state OH radicals interact very strongly.[30] In a recent high level *ab initio* analysis of the transition states on the lowest triplet H_2O_2 potential surface, Karkach *et al.*[31] showed that the barrier for reaction (1) is very small. They determined the electronic energy of the transition state for reaction (1) to be 0.070 eV above the electronic energy of two separated hydroxyl radicals and the van der Waals minimum in the entrance channel, corresponding to a weakly bound hydroxyl radical dimer, to be 0.162 eV below it.

The experiments reported here study the dynamics of reaction (1) using PPC spectroscopy to prepare the system in the transition-state region by photodetachment of the $O^-(H_2O)$ anion and subsequently determining the asymptotic partitioning of energy among the products. These experiments build on the previous transition-state spectroscopy photodetachment experiments of Arnold *et al.*[20] In their experiment, the photoelectron spectra recorded for $O^-(H_2O)$ and its deuterated analog were interpreted in terms of photodetachment of a single isomer of the anion. The photoelectron spectra were observed to change considerably upon deuteration, suggesting that motion of a hydrogen atom orthogonal to the reaction coordinate was responsible for the observed structure, confirmed by one-dimensional simulation of the photoelectron spectra based on *ab initio* potentials.[20] The present experiments reveal vibrationally resolved total translational energy distributions in the dissociative photodetachment of $H_2O_2^-$ and $D_2O_2^-$ and the dissociation energy D_0 $[O^-(H_2O)\rightarrow O^-+H_2O]$. *Ab initio* and density functional calculations on both the anionic and neutral surfaces and two-dimensional wave packet dynamics simulations of the observed photoelectron spectra on model potential energy surfaces are also presented.

II. EXPERIMENT

In these experiments, the DPD of $H_2O_2^-$ was studied by a coincidence measurement of the three photoproducts (electron+two neutral fragments). The experimental method has been previously described in detail[32,33] and will be only briefly reviewed here. A fast beam of mass-selected negative ions ($H_2O_2^-$) was intersected with a pulsed laser beam and the kinematic properties of the photoelectron and neutral fragments were measured in coincidence. The apparatus consists of a mass-selected anion source, a photoelectron spectrometer, and a photofragment translational spectrometer. High detection efficiencies and use of time and position-sensitive particle detectors for both the photoelectron and molecular fragments allow the correlated measurement of the kinetic energy of all the products.

$H_2O_2^-/D_2O_2^-$ was generated by crossing a pulsed supersonic expansion of H_2O/D_2O vapor seeded in N_2O with a 1 keV electron beam. Anions are formed in this source through secondary electron attachment and three-body stabilization,[34] and cooled in the expansion to a vibrational temperature of $\approx$450 K.[35] The anions passed through a skimmer into a dif-

ferentially pumped chamber where they were accelerated to beam energies of 2.5 or 4 keV. Two beam energies were used to rule out formation of any long-lived (μs) neutral complexes. After acceleration, the ion beam was referenced to ground potential using a pulsed high voltage switch and the anions were separated according to mass by time of flight (TOF). Fast neutral particles were removed by guiding the ion beam over a beam block situated on the beam axis.

Anions at $m/e=34$ ($H_2O_2^-$) or $m/e=36$ ($D_2O_2^-$) were intersected at a right angle by the third harmonic (258 nm) of a pulsed Ti:Sapphire fundamental (1.2 ps FWHM) generated by a CPA2000 regenerative amplifier (Clark-MXR, Inc.). The laser was focused to a 0.5 mm diameter spot at the interaction region to give a fluence of $\approx$5–10 mJ/cm^2 per pulse. The **E** vector of the linearly polarized output was parallel to the direction of the ion beam in all experiments. Photodetached electrons were detected by one of two time- and position-sensitive wedge-and-strip-anode electron detectors placed opposite each other and perpendicular to the ion beam. Measurement of the electron recoil angle in this experiment is essential to allow correction for both the Doppler broadening due to the fast ion beam and the actual flight path in the large-solid-angle detector. With these corrections, the electron kinetic energy in the center-of-mass (CM) frame (eKE) was determined. The photoelectron spectrometer has been shown to have an effective angular acceptance of $\sim$20% of $4\pi sr$, with a resolution in eKE of $\sim$5% $\Delta E/E$ at 1.3 eV.[33]

Residual ions remaining in the beam after the interaction region were electrostatically deflected out of the beam path to an ion detector, providing the TOF mass spectrum of the negative ions and a means of monitoring the ion beam intensity. Neutral photofragments recoiled out of the beam over a 104 cm flight path and impinged on a time- and position-sensitive multi-particle detector.[33] Given the parent mass and beam velocity, this information yielded the photofragment mass ratio, CM translational energy (E_T) and recoil angles. The photofragment mass resolution is not sufficient, however, to resolve O+D_2O from OD+OD products. An E_T resolution of $\sim$10% $\Delta E/E$ at 0.7 eV has been demonstrated in studies of the photodissociation of O_2^-.

In these experiments, the correlated kinetic energy and angular distribution of the products are recorded directly. All events that produce one electron and two neutral photofragments were analyzed as correlated information for DPD, yielding the $N(E_T,\text{eKE})$ correlation spectrum. Statistics based on spectrometer efficiency and count rate of the experiment ensure that the photoelectron and photofragments from each event are correlated. Under the conditions of this experiment, a typical event rate of 0.13 per laser shot resulted in false coincidences of $\approx$2%.[36]

III. RESULTS

A. Photoelectron-photofragment kinetic energy correlation: $H_2O_2^-$ and $D_2O_2^-$

The $N(E_T,\text{eKE})$ correlation spectrum at 258 nm (4.80 eV) for $H_2O_2^-$ and $D_2O_2^-$ are shown in Figs. 2(a) and 2(b), respectively, as a two-dimensional histogram of the correlation between E_T along the *x*-axis and eKE along the *y*-axis. The one-dimensional $N(E_T)$ and $N(\text{eKE})$ spectra shown are obtained by integrating the correlation spectra over the complementary variable, and represent the distributions measurable in a conventional noncoincidence experiment. The $N(\text{eKE})$ spectrum along the *y*-axis shows broad irregularly spaced features, which reproduce at lower resolution the published photoelectron spectra by Arnold *et al.* at 266 nm.[20] As noted by Arnold *et al.*, the peak positions and intensities in the photoelectron spectrum change upon deuteration. This indicates that the observed peaks are related to hydrogen motion of the neutral complex formed by photodetachment.

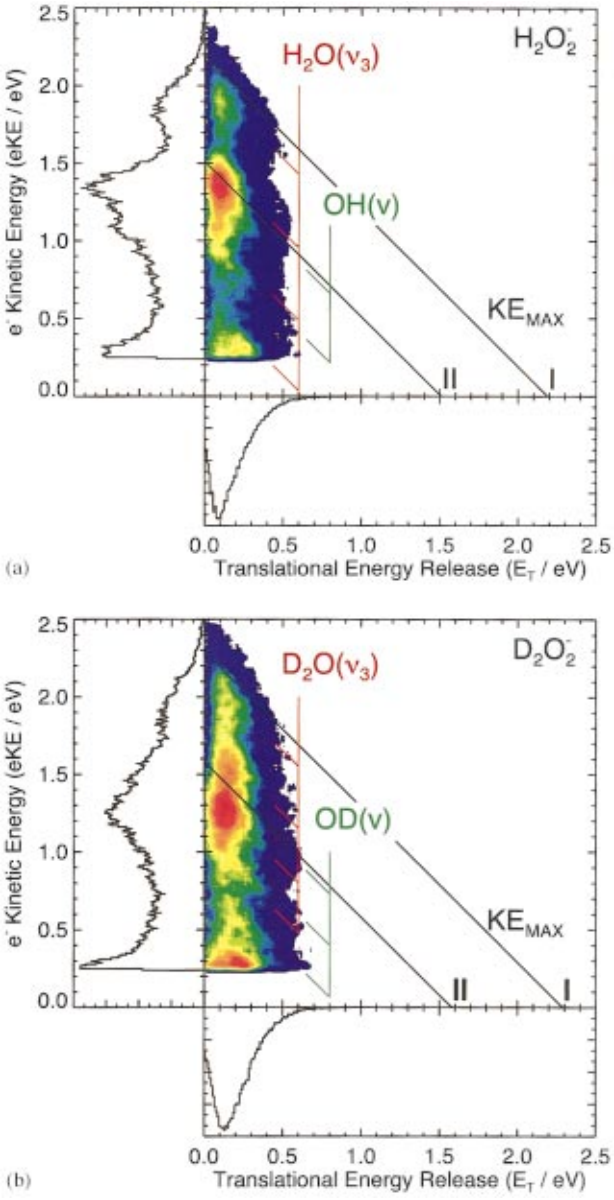

FIG. 2. (Color) Photoelectron-photofragment energy correlation spectrum $[N(E_T,\text{eKE})]$ for $H_2O_2^-$ (a) $D_2O_2^-$ (b) at 258 nm. The $N(E_T,\text{eKE})$ spectra are represented as two-dimensional false color histograms, with increasing intensity from blue to red. The diagonal lines marked KE_{MAX} represent the maximum translational energy in the O+H_2O+e^- product channel, while the diagonal line marked II represents the maximum translational energy for OH+OH+e^-. Diagonal combs showing energetically allowed H_2O ν_3 and OH vibrations are also shown.

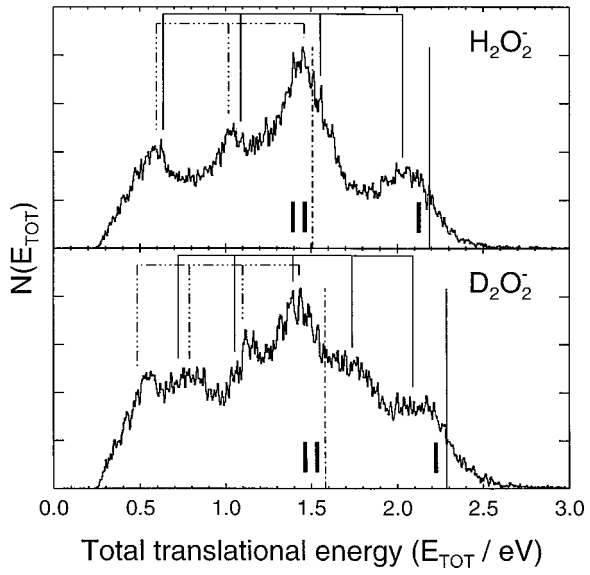

FIG. 3. Vibrationally resolved product translational energy $[N(E_{\mathrm{TOT}})]$ spectra for the DPD of $H_2O_2^-$ and $D_2O_2^-$ at 258 nm as labeled. The full lines represent the dissociation asymptotes into $O+H_2O$ (I) and $O+D_2O$ (I) marked as KE_{MAX} in Figs. 2(a) and 2(b), respectively. The dashed lines represent the dissociation asymptotes into the entrance channel OH+OH (II) and OD+OD (II), respectively. Combs corresponding to the vibrational states of the products are shown as in Fig. 2.

The $N(E_T)$ spectra, which provide a measure of the photofragment repulsion, exhibit broad peaks centered near $E_T \approx 0.10$ eV for the H_2O_2 system and shift to higher kinetic energy $E_T \approx 0.14$ eV upon deuteration.

Correlation of the broad peaks in the $N(\mathrm{eKE})$ and $N(E_T)$ spectra reveals a series of faint diagonal bands. All events that lie within a single diagonal band are characterized by a well-defined total kinetic energy ($E_{\mathrm{TOT}}=E_T+\mathrm{eKE}$) because of energy conservation. Within a band, however, there is a range of kinetic energy partitioning between the three products (electron and two photofragments). The maximum translational energy, corresponding to the $O(^3P)+H_2O$ product channel, is defined by:

$$KE_{\mathrm{MAX}}=h\nu-D_0(H_2O_2^-)-EA(O), \tag{3}$$

where $h\nu=4.80$ eV is the laser energy, D_0 is the bond dissociation energy $H_2O_2^-\rightarrow O^-+H_2O$ or $D_2O_2^-\rightarrow O^-+D_2O$, and $EA(O)=1.462$ eV is the electron affinity of oxygen.[37] This limit represents the dissociation asymptote in the exit channel (I) and is marked as KE_{MAX} in Figs. 2 and 3. KE_{MAX} is drawn at the same contour level (15%) as for the previously studied $H_3O_2^-$ and $D_3O_2^-$, where the bond dissociation energy has been accurately measured,[2] yielding KE_{MAX} $(H_2O_2^-)=2.19\pm0.08$ eV and KE_{MAX} $(D_2O_2^-)=2.29\pm0.08$ eV at 258 nm. From Eq. (3) we derive the bond dissociation energies $D_0(H_2O_2^-\rightarrow O^-+H_2O)=1.15\pm0.08$ eV and $D_0(D_2O_2^-\rightarrow O^-+D_2O)=1.05\pm0.08$ eV, assuming that the KE_{MAX} limits correspond to ground-state neutral products produced from ground-state anions.

The lower bond dissociation energy in the deuterated case indicates that the change in the zero point energy ($\Delta\Delta ZPE=0.10$ eV) in the bound anion complex is smaller than $\Delta\Delta ZPE$ in the separated O^- and H_2O fragments upon deuteration. This behavior is similar to the $H_3O_2^-/D_3O_2^-$ system where we found a $\Delta\Delta ZPE$ of 0.15 eV.[2] The dissociation asymptotes (II) in the entrance channel leading to 2OH or 2OD are drawn 0.68 and 0.71 eV below KE_{MAX} for $H_2O_2^-$ and $D_2O_2^-$, respectively. This value corresponds to the exothermicity of reaction (1).[4,5]

The dominant features observed in the $N(E_T,\mathrm{eKE})$ spectra are a series of four faint diagonal bands for $H_2O_2^-$ and six faint diagonal bands for $D_2O_2^-$. To provide a point of reference, diagonal combs showing the asymmetric stretch (ν_3) states of the water and the vibrational states of the hydroxyl radical are shown on both figures. The simplest explanation of these features is that they correspond to dissociative photodetachment (DPD) onto vibrationally adiabatic curves as found in the $H_3O_2^-$ system.[2] As discussed below, these adiabatic curves are located around the transition state for the neutral bimolecular reaction, and they correlate with the different vibrational states of the OH+OH products in the entrance or $O+H_2O$ products in the exit channel. Examination of the E_T distribution for each correlation band shows some variation, and may represent an important observable for comparison with future dynamics calculations. This observation is consistent with the interpretation that these diagonal ridges correspond to different adiabatic curves in the transition state region correlated with the various product vibrational states, with some variation in slope relative to the asymptotic product channels. Thus in this half-collision experiment we directly probe the vibrational thresholds for the bimolecular reaction by measuring the photoelectrons and photofragments in coincidence.

B. Total kinetic energy release spectra of $H_2O_2^-$ and $D_2O_2^-$ at 258 nm

Another way to view the correlated $N(E_T,\mathrm{eKE})$ data is by direct examination of the total translational energy spectra $N(E_{\mathrm{TOT}})$ generated by summing the photoelectron kinetic energy and the translational energy release for each event: $E_{\mathrm{TOT}}=E_T+\mathrm{eKE}$. The $N(E_{\mathrm{TOT}})$ spectra for $H_2O_2^-$ and $D_2O_2^-$ are shown in Fig. 3, and since evidence for diagonal structure was observed in the $N(E_T,\mathrm{eKE})$ data, these spectra display more resolved structure than the $N(\mathrm{eKE})$ photoelectron spectra alone. The dissociation asymptotes for the exit channels $O(^3P)+H_2O$ or $O(^3P)+D_2O$ (I) which correspond to KE_{MAX} and the entrance channels OH+OH or OD+OD (II) are marked by the vertical lines. In this spectrum, the diagonal bands in the $N(E_T,\mathrm{eKE})$ spectra appear as a resolved spectrum of the correlated product vibrational distribution. A series of combs corresponding to the vibrational states of the products, as in Fig. 2, show a good correlation with the observed features. Examination of the offset of the vibrational peaks from the assigned limits $KE_{\mathrm{MAX}}=2.19$ eV for $H_2O_2^-$ and $KE_{\mathrm{MAX}}=2.29$ eV for $D_2O_2^-$ in this spectra give a sum for the rotational energy and bending excitation in the lowest observed state of the H_2O products of $\approx$160 meV and $\approx$200 meV in D_2O.

If the experiment had higher total translational energy resolution, detailed product state distributions could be extracted from the $N(E_{\mathrm{TOT}})$ spectra. In the $D_2O_2^-$ spectrum,

two vibrational features are visible in the energy range where only $O+D_2O$ products are accessible, which we assign to the asymmetric stretch of the D_2O product based on the *ab initio* calculations discussed below. In the $H_2O_2^-$ spectrum, the first asymmetric stretch of H_2O falls at nearly the same energy as the $2OH(v=0)$ threshold, leading to the large peak in the $N(E_{TOT})$ spectrum at 1.46 eV. It is difficult to extract more detailed product state distributions with the limited resolution observed here.

C. Electronic structure calculations

To aid in the interpretation of these experiments, density functional theory (DFT) and *ab initio* calculations were performed using the GAUSSIAN 98 program package[38] for the anion and neutral complexes involved in these experiments. Complete-active-space self-consistent-field (CASSCF) calculations[39] for the anion complexes were also carried out to characterize the anion potential with the DALTON program package.[40]

1. Anion calculations

For the anion reaction (2), two electronic potential energy surfaces ($^2A'$ and $^2A''$) connect the $OH(^2\Pi_i)$ and $OH^-(^1\Sigma^+)$ reactants to the $O^-(^2P)$ and $H_2O(^1A_1)$ products. The CASSCF calculations were performed using the augmented correlation-consistent polarized-valence-double-zeta (aug-cc-pVDZ) basis set, with the lowest two doubly occupied molecular orbitals (MOs) kept frozen and an active space of 12 MOs used to allocate 15 electrons. The imposed orbital occupation for the $^2A''$ state is $\ldots(6a')^2(1a'')^2(7a')^2(8a')^2(2a'')^1$ and for the $^2A'$ state is $\ldots(6a')^2(1a'')^2(7a')^2(8a')^1(2a'')^2$. The CASSCF calculations on the $O^-(H_2O)$ system considering both electronic states reveal four minima and two connecting transition states very close in energy as detailed in Table I. In agreement with the most detailed theoretical studies of this system[11,20] the $^2A''$ $O^-(H_2O)$ complex was found to be the most stable with a very flat potential energy surface in the proton transfer coordinate between O^- and OH^-. From an energetic point of view, since dynamical correlation was not included, the calculated energy difference between these states is probably not meaningful, and it is likely that both electronic states are populated in the ion beam. DFT calculations by Hrušák *et al.* mentioned above, suggested a very anharmonic single well potential with a shoulder.[11] DFT calculations with the standard Becke3LYP density functional[41] were carried out in order to map the potential in the proton transfer coordinate used in the wave packet dynamics simulations discussed below. These results, for both the anion and the neutral, are given in Table II. Structures of the calculated stationary points for both the anion and the neutral are shown in Fig. 4.

2. Neutral calculations

In reaction (1) the interaction of two ground state $OH(^2\Pi_i)$ radicals leads to four singlet and four triplet states.[42] The hydroxyl radical disproportionation (1) can occur adiabatically on three of the four triplet surfaces along a planar C_s reaction path. Based on the CASSCF calculations of the $O^-(H_2O)$ anion, one-electron photodetachment from either of the low-lying $^2A'$ and $^2A''$ electronic states of the anion can form the $^3A'$ and $^3A''$ states separated by ~2.4 kcal/mol, with the $^3A''$ state lower in energy.[42] Calculations using DFT were carried out but are not reliable due to problems with the energetics using the B3LYP functional and the 6-311++G(3*df*,2*p*) basis set. Instead, we used the energetics obtained from QCISD(T)/6-311++G(3*df*,2*p*) single point calculations[43] for scaling the barrier height on the semi-empirical LEPS surface used in the time-dependent wave packet calculations discussed below. These results are collected in Table III, with the resulting calculated energetics presented in Table IV. The energetics in Table IV were computed using the QCISD electronic energies in conjunction with the zero-point energy corrections from the DFT calculations in Table II, and show generally good agreement with experimental values. More extensive quantum chemical calculations on this difficult system are beyond the scope of the present study. One important result of these and earlier calculations on this system is that the bond length between O_b and H_b (the terminal hydrogen atom) is very close to that in free H_2O, suggesting that excitation of the asymmetric stretch in the water product dominates. The transition state on the neutral surface is also found to be more bent ($\angle O_aH_aO_b = 141°$ at the transition state as opposed to 178° in the $O^-(H_2O)$ well at the DFT level of theory), suggesting that bending excitation in the dynamics on the neutral surface may be important.

TABLE I. Optimized geometries (bond lengths in Å, angles in degrees), electronic energies (Hartrees), zero point energies (Hartrees per particle), and total energies (electronic energy+zero point energy) of the stationary points along the reaction path for the $OH+OH^-\rightarrow O^-+H_2O$ reaction in the anion [CASSCF(15/12)aug-ccpVDZ].

	$O^-(H_2O)$	$[O–H–OH]^-$–TS	$OH^-(OH)$
$^2A''$			
$O_a–H_a$	1.655	1.21	1.064
$H_a–O_b$	1.031	1.273	1.51
$O_b–H_b$	0.967	0.967	0.972
$\angle O_aH_aO_b$	174.7	179.3	177.7
$\angle H_aO_bH_b$	100.0	103.0	107.0
electronic energy	−151.011 202	−151.006 791	−151.007 802
zero point energy	0.022 469	0.016 955	0.019 614
total energy	−150.988 733	−150.989 836	−150.988 188
$^2A'$			
$O_a–H_a$	1.682	1.213	1.063
$H_a–O_b$	1.028	1.281	1.540
$O_b–H_b$	0.967	0.970	0.972
$\angle O_aH_aO_b$	175.4	179.0	177.8
$\sigma H_aO_bH_b$	100.6	104.2	110.0
electronic energy	−151.009 879	−151.004 717	−151.006 025
zero point energy	0.022 594	0.016 940	0.019 721
total energy	−150.987 285	−150.987 777	−150.986 304

D. Time-dependent wave packet simulations

Arnold *et al.* analyzed the photoelectron spectra obtained for this system in terms of a one-dimensional Franck–

TABLE II. DFT/B3LYP optimized geometries (units as in Table I), vibrational frequencies (cm^{-1}), electronic energies (Hartrees), and zero point energies (ZPE) (Hartrees per particle) of the stationary points in the neutral and anion.

Species (state)	Parameter	This work (B3LYP/ 6-311++G(3*df*,2*p*))	Arnold *et al.* (Ref. 20)
$OH(^2\Pi)$	O–H	0.9739	
	frequency	3722	
	ZPE	0.008 480	
	electronic energy	−75.765 639 9	
$OH^-(^1\Sigma)$	O–H	0.964	
	frequency	3766	
	ZPE	0.008 580	
	electronic energy	−75.830 312 3	
$H_2O(^1A_1)$	O–H	0.961	
	H–O–H	105.2	
	frequencies	1627, 3821, 3925	
	ZPE	0.021 357	
	electronic energy	−76.463 374 5	
$O^-(H_2O)(^2A'')$	O_a-H_a	1.460	1.428
	H_a-O_b	1.077	1.083
	O_b-H_b	0.950	0.964
	$<O_aH_aO_b$	177.7	176.3
	$<H_aO_bH_b$	103.5	102.8
	frequencies	338, 560, 1164, 1550, 3864	
	ZPE	0.021 316	
	electronic energy	−151.655 151 7	
$OH\cdot(OH)(^3A'')$	O_a-H_a	0.976	
van der Waals complex	H_a-O_b	2.033	
	O_b-H_b	0.973	
	$\angle O_aH_aO_b$	177.0	
	$\angle H_aO_bH_b$	175.9	
	frequencies	56, 138, 183, 423, 3692, 3734	
	ZPE	0.018 739	
	electronic energy	−151.535 966 8	
$[OHOH]^{\ddagger}(^3A'')$	O_a-H_a	1.060	1.16
transition state	H_a-O_b	1.310	1.22
	O_b-H_b	0.969	0.96
	$\angle O_aH_aO_b$	140.9	153.3
	$\angle H_aO_bH_b$	110.3	106.9
	frequencies	*i*795, 343, 432, 749, 2054, 3790	···
	ZPE	0.016 785	
	electronic energy	−151.537 101 5	

Condon analysis and assigned the observed features to the O–H–O antisymmetric stretch motion of the transferred hydrogen in the dissociative [O–H–OH] complex.[20] In the present study, we extend this treatment to a two-dimensional time-dependent wave packet simulation of the photoelectron spectra. Given an initial anion wave function and the potential energy surface for the neutral bimolecular reaction, one can simulate the photoelectron spectrum and compare the

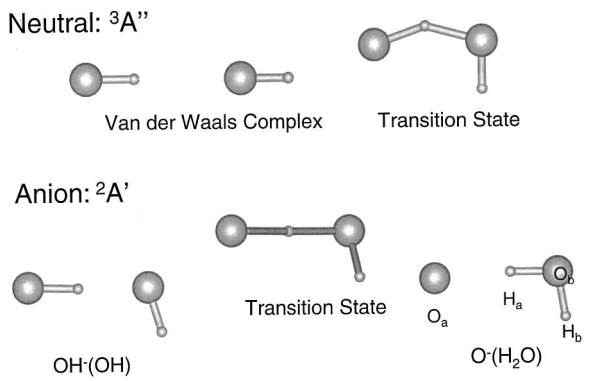

FIG. 4. Calculated [B3LYP/6-311++G(*d*,*p*)] stationary points for the neutral OH+OH system and the CASSCF stationary points for $H_2O_2^-$. Structural parameters are given in Tables I and II.

TABLE III. Electronic energies (Hartrees) found in (U)QCISD(T) calculations of the anion and neutral complexes.

Structure	UQCISD(T)/ 6-311++G(3*df*,2*p*)
$O(^3P)$	−74.994 222 6
$O^-(^2P)$	−75.039 779 5
$OH(^2\Pi_i)$	−75.659 757 2
$OH^-(^1\Sigma_g)$	−75.719 547 7
$H_2O(^1A_1)$	−76.355 346 2
OH^-+OH ($^2A''$) supermolecule	−151.379 198 5
O^-+H_2O ($^2A''$) supermolecule	−151.395 041 6
$O^-(H_2O)$ ($^2A''$) complex	−151.435 635 9
OH+OH ($^3A''$) supermolecule	−151.319 514 9
$O+H_2O$ ($^3A''$) supermolecule	−151.349 568 8
$OH\cdot(OH)$ ($^3A''$) vdW complex	−151.324 951 4
$[OHOH]^{\ddagger}$ ($^3A''$) transition state	−151.315 270 5

TABLE IV. Electron affinities (EA), reaction energies (ΔE_r), barrier height (E_e), association energy (E_{as}), and the anion dissociation energy (D_0), all in eV. Calculated from the QCISD(T) electronic energies listed in Table III and the zero point corrections listed in Table II.

	Calc. (this work)	Expt.	Previous calc. (Ref.)
EA(O^-)(eV)	1.24	1.462[a]	1.40 (G2)[f]
EA(OH^-)(eV)	1.62	1.825[b]	1.87 (G2)[f]
ΔE_r (eV) $OH^-+OH\rightarrow O^-+H_2O$	−0.32	−0.353[c]	0.37 (B3LYP)[f]
D_0 (eV) $O^-(H_2O)\rightarrow O^-+H_2O$	1.11	1.15[d]	1.15 (B3LYP)[f]
ΔE_r (eV) $OH+OH\rightarrow O+H_2O$	−0.70	−0.684[e]	—
E_{as} (eV) $OH+OH\rightarrow OH\cdot(OH)$	0.15	—	0.162[g]
E_e(eV)	0.12	—	0.007[g]

[a]Reference 37.
[b]Reference 12.
[c]Reference 5.
[d]This work.
[e]Reference 4.
[f]Reference 11.
[g]Reference 31 (electronic energy).

results to experiment.[44,45] This approach has been taken on a number of the other transition-state systems experimentally studied by Neumark and co-workers, including FH_2^-,[46] $OHCl^-$,[47] OHF^-,[48] and H_3O^-,[49] providing important insights into the properties of the potential energy surface in the vicinity of the transition state for the neutral bimolecular reaction.

Simulation of the photoelectron spectra using the time-dependent wave packet propagation technique on model potential energy surfaces can provide a qualitative understanding of the region of the potential energy surface probed by these experiments. These simulations use the dynamical wave packet formalism developed by Heller[50] in concert with the wave packet propagation algorithm of Kosloff and Kosloff[51] as implemented by Bradforth *et al.*[44] Upon photodetachment, the anion wave function is projected onto the neutral potential energy surface, giving the starting point for the propagation. The initial wave packet $|\phi(0)\rangle$ propagates as

$$|\phi(t)\rangle = \exp(-i\hat{H}t/\hbar)|\phi(0)\rangle, \tag{4}$$

where $\exp(-i\hat{H}t/\hbar)$ is the time evolution operator and $\hat{H}$ is the nuclear Hamiltonian for the neutral surface. The time autocorrelation function $C(t)$ is defined by the overlap of $|\phi(t)\rangle$ and $|\phi(0)\rangle$:

$$C(t) = \langle \phi(0)|\phi(t)\rangle \tag{5}$$

and the Fourier transform of the autocorrelation function yields the photoelectron spectrum:

$$\sigma(E) \propto \int_{-\infty}^{\infty} \exp(iEt/\hbar)C(t)dt. \tag{6}$$

In future efforts, it will be of interest to extend these calculations to include the product translational and internal state distributions that the coincidence experiments reported here provide, as previously illustrated for the OHF system.[48]

These simulations are restricted to two dimensions, the asymmetric and symmetric stretching motions of the O–H–O moiety, and assume that all nuclear motion occurs on a collinear potential energy surface. While a complete *ab initio* potential energy surface would be desired, this was beyond the scope of the present work, so the semi-empirical London, Eyring, Polanyi, Sato (LEPS) surface was adopted.[52] We consider only the lowest surface of $^3A''$ symmetry, but since the simulations are done in the collinear approximation, the electronic state is $^3\Pi$ for the $OH(^2\Pi)+OH(^2\Pi)\rightarrow O(^3P)+H_2O$ reaction. We constructed a collinear LEPS surface using the parameters listed in Table V, to account for $\Delta E_e = -0.81$ eV for $OH+OH\rightarrow O+H_2O$ and an activation barrier of $E_e = 0.12$ eV at an $O_a-H_a-O_b$ distance of 2.37 Å and a H_aO_b distance of 1.31 Å consistent with the DFT and QCISD calculations on the neutral surface.

TABLE V. LEPS parameters for the collinear neutral surface used in the time-dependent wave packet simulations.

	D_e	β	r_e	S
H_2O	5.443	2.110	0.956	0.110
OH	4.643	2.179	0.971	0.110
O–OH	2.878	2.520	1.324	0.250

The initial anion wave packet was generated using an anharmonic Morse function for the ν_3 asymmetric stretch [$r_e(H_a-O_b) = 1.08$ Å, $\omega_e = 1810\ cm^{-1}$, $\omega_e x_e = 350\ cm^{-1}$] found by fitting the DFT/B3LYP energies generated in a calculation at a fixed equilibrium O_a-O_b distance of 2.54 Å. A harmonic function was used for the symmetric stretch ν_1, [$r_e(O_a-O_b) = 2.54$ Å, $\omega_e = 340\ cm^{-1}$], also chosen to be consistent with the DFT calculations of the anion potential energy surface discussed above.

Simulations were done for both the ground-state anion and also anions with one quantum in ν_3 and ν_1, respectively, as illustrated in Fig. 5. The propagations were carried out for 300 fs and were checked for convergence by varying the time-step and grid size.[53] As seen in the simulations for $H_2O_2^-$ and $D_2O_2^-$ shown in Figs. 6(a) and 6(b), the simulations from the ground state of the anion reasonably reproduce the number and spacing of the observed broad features in the photoelectron spectra in both the $O+H_2O$ and $OH+OH$ channels. The theoretical simulations show little broadening except for the highest eKE features. In the figure, the simulations have been convoluted with the experimental resolution for the photoelectron spectrometer. These results are qualitatively consistent with the one-dimensional (ν_3) simulations carried out by Arnold *et al.* for both systems, and the assignment of the dominant features to specific ν_3 levels

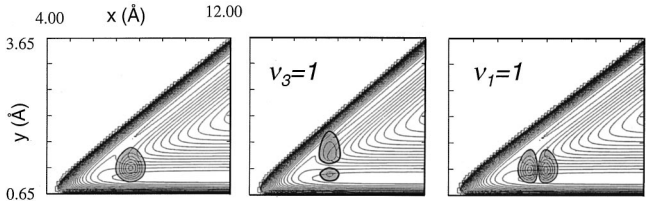

FIG. 5. Initial wave packets (lowest contour contains 90% of the norm of the wave function) on the collinear LEPS potential energy surface (contours at 0.1 eV intervals) for $OH+OH$ $^3A''$ for (a) O–H–OH^- ($\nu_1=0$, $\nu_3=0$); (b) O–H–OH^- ($\nu_1=0$, $\nu_3=1$) and (c) O–H–OH^- ($\nu_1=1$, $\nu_3=0$). The mass-weighted coordinates are $x \approx 3[r(O_a-O_b)]$ and $y = r(H_a-O_b)$ in Å, following Bradforth *et al.* (Ref. 44).

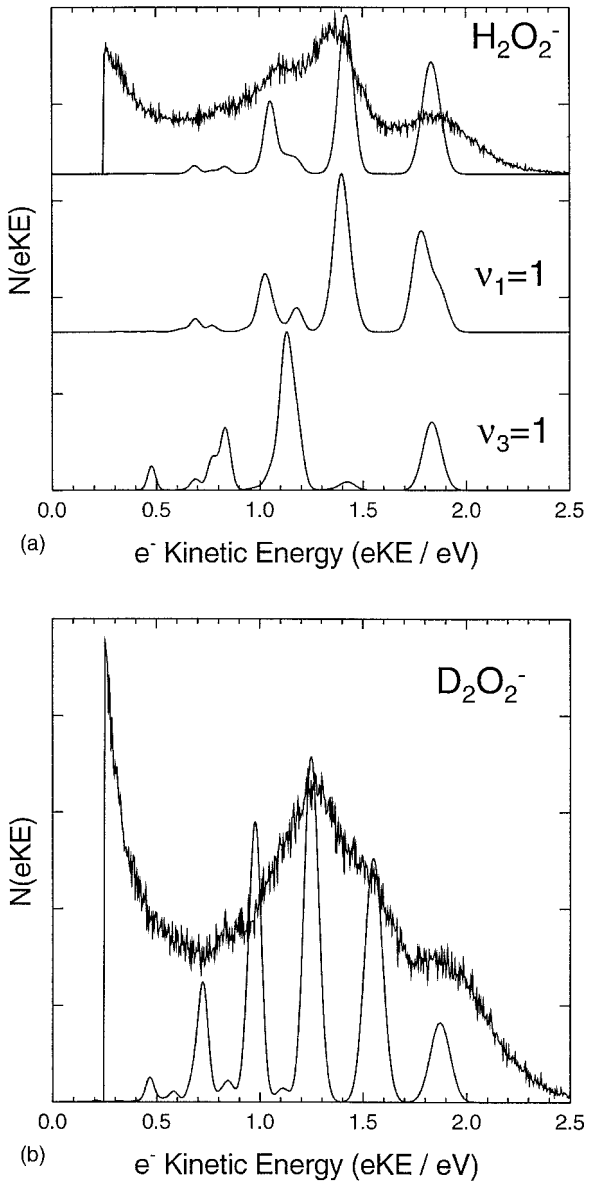

FIG. 6. Simulated photoelectron spectra for (a) $H_2O_2^-$ and (b) $D_2O_2^-$. The top simulation shown in (a) is for $H_2O_2^-$ ($\nu_1=0$, $\nu_3=0$). The middle simulation shows the results for ($\nu_1=1$, $\nu_3=0$), illustrating the preference ν_1 excitation in the anion exhibits for the O+H_2O product channel. The bottom simulation shows the results for ($\nu_1=0$, $\nu_3=1$), illustrating the propensity for ν_3 excitation to produce OH+OH reactants. The simulation in (b) is for $D_2O_2^-$ ($\nu_1=0$, $\nu_3=0$).

on the neutral surface is discussed in their work.[20] Since these time-dependent simulations explicitly include the dissociative reaction coordinate they might be expected to reproduce the widths of the experimental features, however, they are found to be much narrower than observed experimentally.

Simulations for the vibrationally excited anions are also shown for $H_2O_2^-$ in Fig. 6(a), illustrating how excitation of one quantum in ν_1 couples strongly with the O+H_2O product channel, while one quantum in ν_3 predominantly yields the OH+OH entrance channel. This control of product channel by parent vibrational excitation is similar to that previously predicted by Bradforth *et al.* for the Br+HI system,[44] and shows that dissociative photodetachment of $H_2O_2^-$ provides a promising system for demonstrating vibrational state control of product branching ratios.

IV. DISCUSSION

The data presented here provide detailed experimental insights into the half-collision dynamics in the dissociative photodetachment (DPD) of $H_2O_2^-$ and $D_2O_2^-$. Figure 5 shows the mass-weighted two-dimensional potential energy surfaces used to model the neutral surface. The projection of the anion wave functions shown in this figure illustrate that these experiments directly probe the region of the PES near the transition state for the OH+OH→O+H_2O reaction. The observation of diagonal structure in the $N(E_T,\text{eKE})$ spectra and the corresponding vibrationally resolved $N(E_{\text{TOT}})$ spectra provide evidence for significant vibrational adiabaticity in this system, wherein excitation induced by photodetachment is carried over into the final product states.

The total kinetic energy spectra show more structure than the photoelectron spectra in both cases. The photoelectron spectrum [N(eKE)] is determined by the Franck–Condon overlap between the bound anion wave function and the scattering wave function on the neutral surface. A steeply sloped repulsive surface will yield broad features in the photoelectron spectrum due to lifetime broadening. The $N(E_T)$ spectrum is similarly governed by the region of Franck–Condon overlap with the neutral surface, but also by any subsequent transfer of energy from internal to external degrees of freedom in the dissociation process. The total kinetic energy release $E_{\text{TOT}}=E_T+\text{eKE}$ for any given event, however, is determined solely by energy conservation. Thus for a given DPD event the partitioning of the total available energy provides a measure of the resulting product internal state distribution after the DPD process. In the case where the dissociation dynamics of the neutral H_2O_2 system are vibrationally adiabatic, as revealed by the diagonal structure observed in the PPC spectrum shown in Fig. 2, each peak in the photoelectron spectrum correlates experimentally to a product vibrational level in the exit or entrance channel.

The degree of vibrational adiabaticity observed in this hydrogen exchange reaction can be understood in terms of the potential energy surface in mass-weighted coordinates, as discussed previously by Neumark and co-workers for a number of systems.[1,44] As discussed above, the *ab initio* calculations for the anion potential show that the O–H–O atoms are almost linearly arranged, with a spectator H atom attached to one of the O atoms. To a first approximation the outer OH group in the O–H–OH system can be seen as a spectator. For triatomic linear molecules, the skew angle on the mass-weighted potential energy surface is given by $\tan^{-1}[(m_b(m_a+m_b+m_c))/(m_am_c)]^{1/2}$. Using $m_b=1$ (H) and $m_a=16$ (O) and $m_c=17$ (OH) the resulting skew angle is 19.5° while for O–D–(OD) it is found to be 26.6° in a linear configuration of the oxygen atoms and the transferred hydrogen atom. Thus the asymmetric stretch coordinate is nearly orthogonal to motion along the reaction coordinate and is additionally stabilized by an inward force from the potential barrier between the reactant and product valleys. These factors result in a very weak coupling between the asymmetric stretch and

the dissociation coordinate giving rise to the structure dominated by motion of the transferred H-atom, and a strong correlation between the asymmetric stretch states and the reactant and product vibrational states.

The two-dimensional time-dependent simulations of the photoelectron spectra presented here are chiefly of value in a qualitative sense. They are consistent with the previous one-dimensional simulations of Arnold *et al.*,[20] confirming the important role played by the asymmetric stretch states of the neutral complex. The difficulties associated with calculating potential energy surfaces for both the anion and the neutral in this system precluded comparison with more realistic potentials. In addition, the restriction to two degrees of freedom, the assumption of a collinear reactive surface and the concomitant neglect of bending and rotational corrections are all potential reasons for the prediction of narrow features in the photoelectron spectrum. Bending corrections in the time-dependent simulations when using a LEPS surface[44] were evaluated but made little difference in the simulations, so are not presented. Finally, as the simulations show, vibrational excitation in the anion can lead to significant changes in the photoelectron spectra and the product branching ratio. In these experiments anions are produced and cooled in a supersonic expansion, but high frequency modes like the asymmetric stretch of the anion are often characterized by temperatures ≈450 K, so a few percent of the anions can be vibrationally excited as well.

Thus a number of inhomogeneous effects may be dominating the lifetime of the neutral states accessed by photodetachment. It would be of great interest to carry out these experiments at higher energy resolution to observe directly the homogeneous broadening of these states. The width of the $N(E_T)$ distributions and the observation of the diagonal bands in the $N(E_T, \mathrm{eKE})$ correlation spectra suggest that the lifetimes may in fact be much shorter than predicted by the time-dependent simulations carried out here.

V. CONCLUSION

This paper reports a PPC study of the transition-state dynamics of the $OH+OH \rightarrow O(^3P)+H_2O$ reaction using the dissociative photodetachment of $H_2O_2^-$ and $D_2O_2^-$. Although the product channels cannot be cleanly resolved by photofragment mass in either system in these experiments, a bond dissociation energy for the anion is determined, defining the energetics and showing that when the $OH+OH+e^-$ DPD channel is accessible a considerable enhancement in signal intensity is observed. *Ab initio* and DFT calculations were used to characterize the anion surface near the equilibrium geometry and to provide parameters for scaling a collinear O–H–OH LEPS surface for the reaction.

Two-dimensional wave packet simulations give reasonable agreement with the positions and intensities of the observed photoelectron spectra and also demonstrate the strong sensitivity of the product branching ratio on vibrational excitation of the parent anion. Experimentally, higher-resolution coincidence experiments making use of tunable-laser photodetachment and threshold photoelectron detection will be of interest to examine the lifetimes of the dissociating states. Due to the multiple interacting potential energy surfaces in both the anion and the neutral, the $H_2O_2^-/H_2O_2$ system represents a significant challenge to theory, but it is hoped that the results presented here will encourage further studies of this prototypical radical–radical four atom reaction.

ACKNOWLEDGMENTS

This work was supported by the Department of Energy (DOE) under Grant No. DE-FG03-98ER14879. H.J.D. gratefully acknowledges partial support from a Forschungsstipendium sponsored by the Deutsche Forschungsgemeinschaft (DFG) and the DOE. T.G.C. and A.K.L. were supported under AFOSR Grants No. AASERT F49620-97-1-0387 and F49620-96-1-0220. R.E.C. is a Camille Dreyfus Teacher-Scholar, an Alfred P. Sloan Research Fellow and a Packard Fellow in Science and Engineering. We also acknowledge Professor S. E. Bradforth for providing the time-dependent wave packet code and helpful discussions. We thank the National Energy Research Scientific Computing Center (NERSC) for providing computation time.

[1] (a) D. M. Neumark, Acc. Chem. Res. **26**, 33 (1998); (b) R. B. Metz, S. E. Bradforth, and D. M. Neumark, Adv. Chem. Phys. **81**, 1 (1992).
[2] H.-J. Deyerl, A. K. Luong, T. G. Clements, and R. E. Continetti, Faraday Discuss. **115**, 147 (2000).
[3] R. Atkinson, Chem. Rev. **17**, 227 (1998).
[4] B. Ruscic, D. Feller, D. A. Dixon, K. A. Peterson, L. B. Harding, R. L. Asher, and A. F. Wagner, J. Phys. Chem. A **105**, 1 (2001).
[5] M. W. Chase, C. A. Davies, J. R. Downey, D. J. Frurip, R. A. McDonald, and A. N. Syverud, J. Phys. Chem. Ref. Data Suppl. **14**, 1 (1985) (JANAF Tables).
[6] J. Warnatz, in *Combustion Chemistry*, edited by W. C. Gardiner, Jr. (Springer, New York, 1984).
[7] J. A. Miller and C. T. Bowman, Prog. Energy Combust. Sci. **15**, 287 (1989).
[8] K.-H. Gericke, F. J. Comes, and R. D. Levine, J. Chem. Phys. **74**, 6106 (1981).
[9] G. Wagner and R. Zellner, Ber. Bunsenges. Phys. Chem. **85**, 1122 (1981).
[10] World Meteorological Organization, *Global Ozone Research and Monitoring Project*, Report No. 16 (1985).
[11] J. Hrušák, H. Friedrichs, H. Schwarz, H. Razafinjanahary, and H. Chermette, J. Phys. Chem. **100**, 100 (1996).
[12] P. A. Schulz, R. D. Mead, P. L. Jones, and W. C. Lineberger, J. Chem. Phys. **77**, 1153 (1982).
[13] C. Lifshitz, J. Phys. Chem. **86**, 3634 (1982).
[14] J. M. Van Doren, S. E. Barlow, C. H. DePuy, and V. M. Bierbaum, J. Am. Chem. Soc. **109**, 4412 (1987).
[15] M. A. Buntine, D. J. Lavrich, C. E. Dessent, M. G. Scarton, and M. A. Johnson, Chem. Phys. Lett. **216**, 471 (1993).
[16] C. M. Roehl, J. T. Snodgrass, CA. A. Deakyne, and M. T. Bowers, J. Chem. Phys. **94**, 6546 (1991).
[17] S. Humble, I. Demachy, and P. C. Hiberty, Chem. Phys. Lett. **247**, 126 (1995).
[18] S. J. K. Jensen and U. K. Kläning, Chem. Phys. Lett. **241**, 404 (1995).
[19] R. Benassi and F. Taddei, Chem. Phys. Lett. **204**, 595 (1993).
[20] D. W. Arnold, C. Xu, and D. M. Neumark, J. Chem. Phys. **102**, 6088 (1995).
[21] R. Zellner, J. Phys. Chem. **83**, 18 (1979).
[22] E. A. Albers, K. Hoyermann, H. G. Wagner, and J. Wolfrum, 13th Symp. (Int.) on Combustion (The Combustion Institute, 1971), p. 81.
[23] D. Fulle, H. F. Hamann, H. Hippler, and J. Troe, J. Chem. Phys. **105**, 1001 (1996).
[24] Y. Bedjanian, G. Le Bras, and G. Poulet, J. Phys. Chem. A **103**, 7017 (1999).
[25] J. M. Pfeiffer, E. Woods III, R. B. Metz, and F. F. Crim, J. Chem. Phys. **113**, 7982 (2000).
[26] N. Tanaka, U. Nagashima, M. Takayanagi, H. L. Kim, and I. Hanazaki, J.

Phys. Chem. A **101**, 507 (1997); H. Tsurumaki, Y. Fujimura, and O. Kajimoto, J. Chem. Phys. **110**, 7707 (1999); K. Imura, M. Veneziani, T. Kasai, and R. Naaman, *ibid.* **111**, 4025 (1999); R. Sayos, C. Oliva, and M. Gonzalez, *ibid.* **113**, 6736 (2000).
[27] E. P. Dougherty and H. Rabitz, J. Chem. Phys. **72**, 6571 (1980).
[28] U. Maas and J. Warnatz, Combust. Flame **74**, 53 (1988); U. Maas and S. B. Pope, *ibid.* **88**, 239 (1992).
[29] L. B. Harding and A. F. Wagner, 22nd Symp. (Int.) on Combustion (The Combustion Institute, 1988), p. 983.
[30] L. B. Harding, J. Phys. Chem. **95**, 8653 (1991).
[31] S. P. Karkach and V. I. Osherov, J. Chem. Phys. **110**, 11918 (1999).
[32] K. A. Hanold, C. R. Sherwood, M. C. Garner, and R. E. Continetti, Rev. Sci. Instrum. **66**, 5507 (1995).
[33] K. A. Hanold, A. K. Luong, T. G. Clements, and R. E. Continetti, Rev. Sci. Instrum. **70**, 2268 (1999).
[34] M. A. Johnson and W. C. Lineberger, in *Techniques in Chemistry*, edited by J. M. Farrar and W. H. Saunders (Wiley, New York, 1988), Vol. 20, p. 591.
[35] M. C. Garner, K. A. Hanold, M. Sowa Resat, and R. E. Continetti, J. Phys. Chem. A **101**, 6577 (1997).
[36] R. E. Continetti, in *Photoionization and Photodetachment, Adv. Ser. Phys. Chem. Vol. 10B,* edited by C. Y. Ng (World Scientific, Singapore, 2000), pp. 748–808.
[37] H. Hotop and W. C. Lineberger, J. Phys. Chem. Ref. Data **14**, 731 (1985).
[38] M. J. Frisch, G. W. Trucks, H. B. Schlegel *et al.*, GAUSSIAN 98, Revision A.9, Gaussian, Inc., Pittsburgh, PA, 1998.
[39] F. Bernardi, A. Bottini, J. J. W. McDougall, M. A. Robb, and H. B. Schlegel, Faraday Symp. Chem. Soc. **19**, 137 (1984).
[40] T. Helgaker, H. J. Aa. Jensen, P. Joergensen *et al.*, ''Dalton release 1.0 (1997), an electronic structure program.''
[41] A. D. Becke, J. Chem. Phys. **98**, 1372 (1993); *ibid.* **98**, 5648 (1993); C. Lee, W. Yang, and R. G. Parr, Phys. Rev. B **37**, 785 (1988).
[42] L. Harding, J. Phys. Chem. **95**, 8653 (1991).
[43] J. A. Pople, M. Head-Gordon, and K. Raghavachari, J. Chem. Phys. **87**, 5968 (1987).
[44] S. E. Bradforth, A. Weaver, D. W. Arnold, R. B. Metz, and D. M. Neumark, J. Chem. Phys. **92**, 7205 (1990).
[45] R. B. Metz and D. M. Neumark, J. Chem. Phys. **97**, 962 (1992).
[46] D. E. Manolopoulos, K. Stark, H.-J. Werner, D. W. Arnold, S. E. Bradforth, and D. M. Neumark, Science **262**, 1852 (1993).
[47] M. J. Davis, H. Koizumi, G. C. Schatz, S. E. Bradforth, and D. M. Neumark, J. Chem. Phys. **101**, 4708 (1994).
[48] R. N. Dixon and H. Tachikawa, Mol. Phys. **97**, 195 (1999).
[49] W. H. Thompson and W. H. Miller, J. Chem. Phys. **101**, 8620 (1994); D. Wang, J. Z. H. Zhang, and C. Yu, Chem. Phys. Lett. **273**, 171 (1997); D. C. Clary, J. K. Gregory, M. J. T. Jordan, and E. Kauppi, J. Chem. Soc., Faraday Trans. **93**, 747 (1997); M. Igarashi and H. Tachikawa, Int. J. Mass. Spectrom. **197**, 243 (2000).
[50] E. J. Heller, Acc. Chem. Res. **14**, 368 (1981).
[51] D. Kosloff and R. Kosloff, J. Comput. Chem. **52**, 35 (1983).
[52] J. Espinosa-Garcia, J. Phys. Chem. A **105**, 134 (2001).
[53] S. E. Bradforth, Ph.D. Thesis, University of California, Berkeley (1992).